

Redox-tunable isoindigos for electrochemically mediated carbon capture

Received: 26 April 2023

Accepted: 23 January 2024

Published online: 08 February 2024

Xing Li¹, Xunhua Zhao^{2,3}, Lingyu Zhang¹, Anmol Mathur¹, Yu Xu¹, Zhiwei Fang⁴, Luo Gu⁴, Yuan Yue Liu² & Yayuan Liu¹✉

Efficient CO₂ separation technologies are essential for mitigating climate change. Compared to traditional thermochemical methods, electrochemically mediated carbon capture using redox-tunable sorbents emerges as a promising alternative due to its versatility and energy efficiency. However, the undesirable linear free-energy relationship between redox potential and CO₂ binding affinity in existing chemistry makes it fundamentally challenging to optimise key sorbent properties independently via chemical modifications. Here, we demonstrate a design paradigm for electrochemically mediated carbon capture sorbents, which breaks the undesirable scaling relationship by leveraging intramolecular hydrogen bonding in isoindigo derivatives. The redox potentials of isoindigos can be anodically shifted by >350 mV to impart sorbents with high oxygen stability without compromising CO₂ binding, culminating in a system with minimised parasitic reactions. With the synthetic space presented, our effort provides a generalisable strategy to finetune interactions between redox-active organic molecules and CO₂, addressing a longstanding challenge in developing effective carbon capture methods driven by non-conventional stimuli.

Carbon capture from stationary emitters or directly from the ambient environment, followed by sequestration or utilisation, is critical to mitigating climate change^{1–3}. However, the incumbent wet chemical scrubbing methods for carbon dioxide (CO₂) separation are technically and economically challenged by various inherent limitations, including high energy consumption for sorbent regeneration, thermal degradation, complexity in heat integration when retrofitting existing infrastructures, process equipment corrosion, and fugitive emission of volatile toxic sorbents to the environment^{4,5}. Alternatively, electrochemically mediated carbon capture (EMCC) has emerged as a promising technology^{6–11}. In EMCC, reversible CO₂ capture and release is modulated by switching electrochemical potentials. Therefore, they can be operated isothermally at ambient pressure, powered by renewable energy sources, and modularly designed to accommodate the multiscale nature of carbon capture

needs. Among the EMCC mechanisms explored to date, one popular strategy is to use redox-active organic compounds as CO₂ carriers (redox-tunable Lewis bases), with quinones being the most studied class of molecules^{12–14}. Electro-reduction of these molecules generates nucleophiles that form adducts with electrophilic CO₂, which can be later oxidised to liberate pure CO₂ while regenerating the sorbents (Fig. 1a). The past two decades have witnessed steady research progress in developing EMCC processes using redox-tunable sorbents^{8,10,15–20}. Several bench-scale prototypes have been demonstrated for fixed-bed and flow-based CO₂ separations attributed to materials and device-level engineering efforts^{17–19}. In contrast, molecular-level design principles for precise sorbent property tuning remain largely unestablished beyond the simplistic method of structural substitution with electron-donating and withdrawing groups, despite their central role in EMCC.

¹Department of Chemical and Biomolecular Engineering, Johns Hopkins University, Baltimore, MD 21218, USA. ²Department of Mechanical Engineering & Texas Materials Institute, The University of Texas at Austin, Austin, TX 78712, USA. ³Macao Institute of Materials Science and Engineering (MIMSE), Faculty of Innovation Engineering, Macau University of Science and Technology, Taipa, Macau 999078, China. ⁴Department of Materials Science and Engineering, Johns Hopkins University, Baltimore, MD 21218, USA. ✉e-mail: yayuanliu@jhu.edu

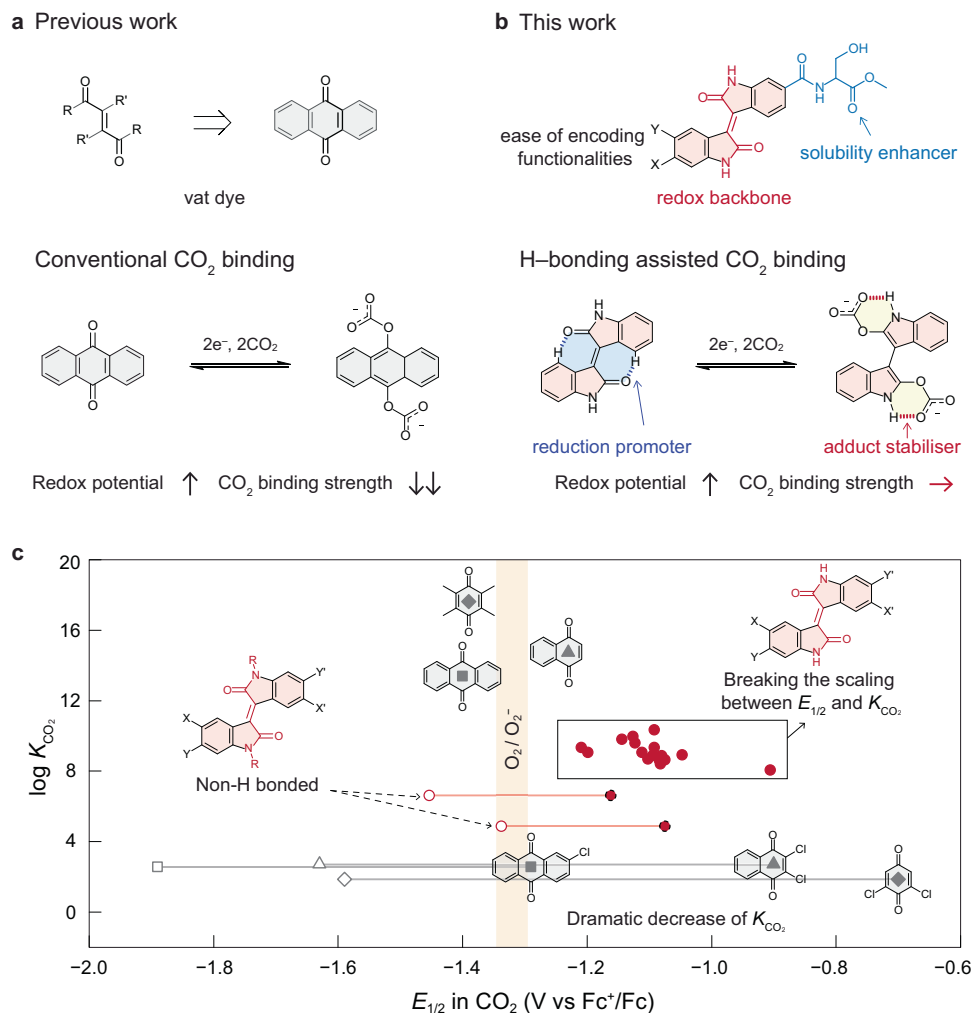


Fig. 1 | Rational design of bifunctional redox-tunable CO₂ sorbents based on isoindigo and their derivatives. **a** A universal designing pattern for redox-tunable CO₂ carriers containing α,β -unsaturated 1,4-diketone functionality. In previous designs, CO₂ is only bonded to the reduced O centre via carbonate formation, where the binding affinity is sensitive to structural modification. **b** Bifunctional redox-tunable CO₂ carrier design based on isoindigo. The secondary functionality

of amide allows intramolecular hydrogen bonding, providing an extra handle to stabilise the CO₂ adduct, thereby enhancing the CO₂ binding strength. **c** A summary of $E_{1/2}$ of typical quinone-based sorbents and isoindigos under CO₂, and their log K_{CO_2} in DMF (filled and empty dots represent the first and second $E_{1/2}$ under CO₂, respectively circle, isoindigos; diamond, benzoquinone; triangle, naphthoquinone; square, anthraquinone).

The lack of reliable sorbent chemistry has intrinsically hindered existing EMCC processes. A practical EMCC system usually requires chemical modification of redox-tunable sorbents to improve key properties such as solubility, processibility, and stability against impurities. For example, anodically shifting the redox potential will enhance the robustness of activated sorbent against molecular oxygen (O₂), a common gas stream impurity, for improved carbon capture efficiency. Nevertheless, the CO₂ binding affinity of existing redox-tunable Lewis base sorbents, such as quinones, is highly susceptible to chemical modifications, which decreases dramatically as the redox potential shifts anodically^{21–23}. The seminal work from W. L. Bell et al. introduced a method to calculate the CO₂ binding constant (K_{CO_2}) of activated sorbent, which is widely adopted later to evaluate the CO₂ binding strength¹². As an example, anthraquinone exhibits a two-electron-transfer half-wave potential ($E_{1/2}$) of -1.4 V vs. ferrocenium/ferrocene (Fc⁺/Fc) in *N,N*-dimethylformamide (DMF) under CO₂ and a log K_{CO_2} of -13.4 (Fig. 1c). The installation of electron-withdrawing groups (EWGs), such as one chloro group at 2-position, can anodically shift $E_{1/2}$ to -1.25 V vs. Fc⁺/Fc, yet the log K_{CO_2} decreased substantially to 2.73 (Fig. 1c and Supplementary Table 1)²¹. A minimum log K_{CO_2} of -3.0 in DMF is required to attain a practical efficiency for point source

carbon capture (10% CO₂), and the log K_{CO_2} must be >-5.5 for atmospheric CO₂ concentration (400 ppm)¹². Importantly, it is challenging to overcome the coupling between $E_{1/2}$ and log K_{CO_2} , as it is dictated by the fundamental principle in chemistry that electron deficiency facilitates reduction but in return weakens nucleophilicity²⁴. Therefore, to fulfil the practical requirements of EMCC, it is pivotal to develop new classes of redox-tunable sorbents that can break the linear free-energy relationship between redox potential and CO₂ binding strength to enable aerobic stability and high CO₂ capacity (Supplementary Fig. 1).

Here, through analysing the structures of existing EMCC sorbents, we observe that the most representative quinoid species share a common pattern of α,β -unsaturated 1,4-diketone (Fig. 1a). Inspired by this structural pattern, we present a class of redox-tunable CO₂ carriers based on isoindigo compounds, which can successfully overcome the undesirable coupling between redox potential and CO₂ binding strength (Fig. 1b, c). With a molecular library of 21 examples and a combined experimental and computational effort, we show that the α,β -unsaturated 1,4-diketone in isoindigos plays the role of redox backbone for CO₂ binding and the amide groups act as extra docking sites for CO₂ complexation via intramolecular hydrogen bonding. This unique bifunctional structural design allows a wide range of chemical

modifications to independently optimise key sorbent properties without sacrificing their abilities for CO₂ binding. The isoindigo family culminates in an EMCC system that can operate at mild potentials (around -1 V vs. Fc⁺/Fc) with log *K*_{CO₂} maintained at -9. The value is five orders of magnitude higher than tetrachloroquinone with alcohol additives²², which is the state-of-the-art sorbent chemistry with an attempt to break the linear free-energy relationship. Flow-based separation prototypes have also been demonstrated to evaluate the EMCC performance of the isoindigo sorbents, which can achieve CO₂ capacity utilisation efficiencies up to ~80% and energy consumptions as low as 127.3 kJ mol⁻¹ per CO₂ capture/release cycle. With intrinsic O₂ stability, high structural tunability, and synthetic feasibility, isoindigos are promising to serve as the next-generation EMCC sorbents. Moreover, this work demonstrates a generalisable strategy to overcome the intrinsic linear free-energy limits in redox-active organic species that can be broadly applied to EMCC and beyond.

Results

Redox-tunable CO₂ absorption of isoindigo

Isoindigo and its derivatives have been extensively utilised as core building blocks in organic semiconductors^{25–28}, but have rarely been explored as redox molecules for organic electrodes. We envisage isoindigos bearing α,β -unsaturated 1,4-diketone functionalities to be redox-active and can complex with CO₂ at the oxygen centres in the reduced state. A series of electrochemical experiments was conducted to validate the redox-driven interaction between isoindigo (Ild) and CO₂. First, we performed bulk electrolysis of Ild using 0.25 M lithium perchlorate (LiClO₄) in dimethyl sulfoxide (DMSO) as the supporting electrolyte under N₂ or CO₂ atmosphere (Fig. 2a). Under N₂, the dark

dispersion of Ild turned greenish at the beginning of the reduction and became a clear yellow solution when the reaction was completed. This suggests the formation of the bisindolidenolate intermediate, which is expected to absorb CO₂ as a Lewis base. Interestingly, the yellow solution quickly turned red when purged with CO₂, implying the formation of the Ild-CO₂ adduct. To our delight, ¹H and ¹³C nuclear magnetic resonance (NMR) spectra of the crude solution confirm the full conversion of Ild into Ild-CO₂ with negligible side products (Fig. 2b). Characteristic peaks for the carbonate carbon were observed at 176–177 ppm in ¹³C NMR. Besides, the proton on the lactam N shifts upfield to 10.33 ppm in Ild-CO₂ compared to that of 10.69 ppm in Ild, strongly evidencing the formation of intramolecular hydrogen bonding with complexed CO₂ (highlighted in red in Fig. 2a). The NMR spectra exhibit two types of amide hydrogens and carbonate carbons, which is probably due to the rotational isomerisation of Ild-CO₂ (Supplementary Fig. 2). The presence of intramolecular hydrogen bonding in Ild-CO₂ was further verified by variable-temperature (VT) ¹H NMR, 2D ¹H-¹³C Heteronuclear Single Quantum Coherence (HSQC) NMR, and Fourier transform infra-red (FT-IR) experiments (Supplementary Figs. 3–5, see Supplementary Note 1 for detailed analysis). The full NMR peak assignment of Ild and Ild-CO₂ is given in Supplementary Fig. 2.

Since the discovery of the EMCC mechanism using quinones in 1988^{12,13}, to our best knowledge, the widely accepted electrochemically generated quinone-CO₂ carbonate adduct is still a proposed structure and has not been confirmed in an EMCC process by non-ambiguous characterisations. This is probably due to the poor stability of the adducts and the transient bonding nature between the reduced sorbent and CO₂. On the contrary, crude NMR spectra suggest bulk

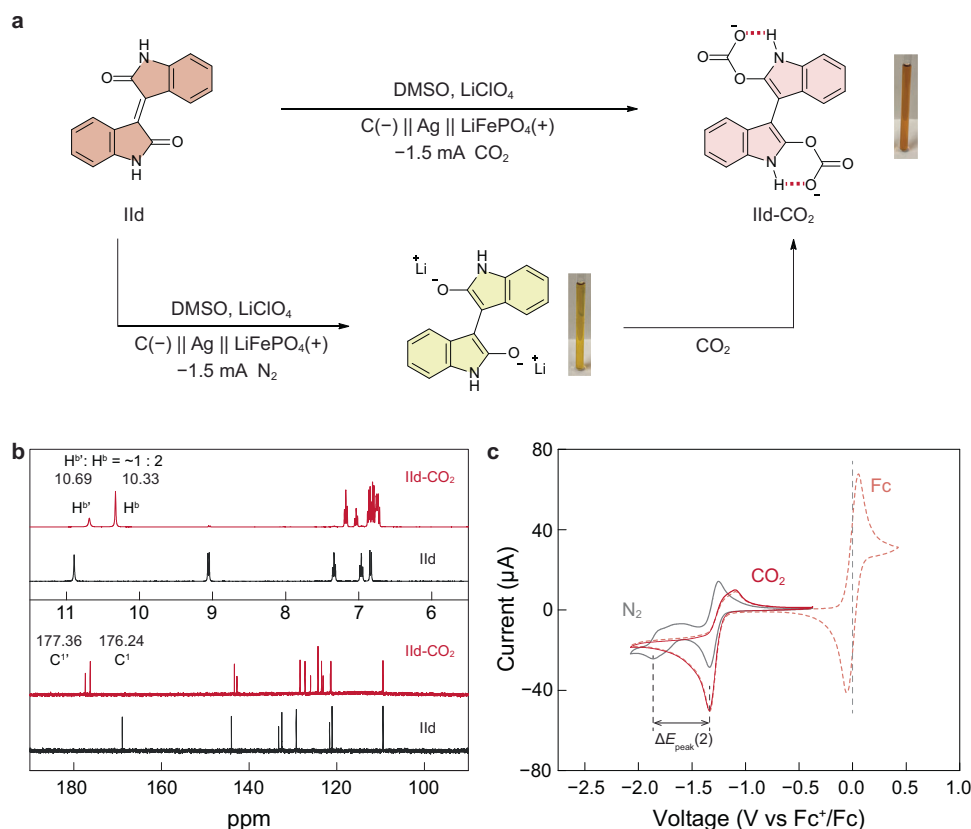


Fig. 2 | Validating the redox-tunable CO₂ absorption of isoindigo. **a** Bulk electrolysis of isoindigo (Ild) under N₂ or CO₂ atmosphere. The CO₂ adduct can be obtained either by directly reducing Ild (40 mM) in DMSO with 0.25 M LiClO₄ under CO₂ or by reducing Ild under N₂ followed by purging with CO₂. **b** ¹H NMR and ¹³C NMR spectra of the crude solution after bulk electrolysis under CO₂. The minor

isomer peaks are marked with an asterisk. **c** CV curves of Ild (2.5 mM) in DMF using 0.1 M Nbu₄PF₆ as the supporting salt under N₂ (grey) and CO₂ (red) at a scan rate of -50 mV s⁻¹ (5 mM ferrocene as the internal reference). $\Delta E_{\text{peak}(2)}$ is labelled for the calculation of *K*_{CO₂}.

electro-reduction of IId under CO₂ can yield the proposed adduct with full conversion (IId was fully consumed), indicating the high selectivity of this chemistry and the sufficient stability of the adduct, which we postulate to be the result of intramolecular hydrogen bonding. Noticeably, the IId-CO₂ solution obtained from bulk electrolysis can be stably stored in ambient air with high water content. After 53 days, <9 mol% of IId-CO₂ oxidised back to the neutral IId form (Supplementary Fig. 6).

To confirm the redox activity of IId, we measured its cyclic voltammetry (CV) using 0.1 M tetrabutylammonium hexafluorophosphate (NBu₄PF₆) in DMF as the supporting electrolyte (Fig. 2c). Under an inert N₂ atmosphere, IId exhibits two major redox waves typical to stepwise two-electron transfer. Like quinoid species¹³, the two electron transfer steps correspond to the formation of anionic radicals (IId^{•-}) and dianions (IId²⁻), respectively. The two reduction peaks under N₂ emerge into one in the presence of CO₂ with a nearly doubled peak current, indicating chemical interactions between reduced IId and CO₂. This behaviour is analogous to the other redox-tunable CO₂ sorbents reported previously based on oxygen or nitrogen binding centres, whose reaction with CO₂ proceeds via an ECEC mechanism (E, electron transfer; C, chemical reaction)^{12,13,20}. As a Lewis acid, CO₂ can withdraw the electron density from IId^{•-} to promote the second electron transfer, giving rise to an anodically shifted second reduction wave. Besides, the oxidation peak also shifts anodically and becomes quasi-reversible, corroborating the formation of the IId-CO₂ adduct, which requires more energy for CO₂ desorption.

This preliminary finding encouraged us to expand the chemical scope of isoindigos and search for more qualified EMCC compounds. Isoindigos can be synthesised through the condensation reaction between 2-oxindoles and isatins. This allows the modular design of redox sorbents, where the two building units can be modified separately and integrated into isoindigos in the last step, thereby addressing the synthetic barriers when engineering EMCC sorbents (Supplementary Note 2). Here, we demonstrate the structural modification of isoindigo at 5, 6, and *N*-positions with 21 examples (Fig. 3) and examine in detail the interplay between substituent groups and hydrogen bonding on the redox and CO₂ binding behaviours of isoindigos to establish the underlying structure-property relationships. The main conclusions are summarised in Fig. 4 and will be discussed in detail in the following sections.

Tuning the redox potential of isoindigos

We first examine the redox behaviours of derivatised isoindigos under N₂ via CV. Delightfully, all the isoindigos tested display redox couples typical to stepwise two-electron transfer, underscoring the good electrochemical reversibility of these molecules (Fig. 4a, Supplementary Figs. 7–9).

Among the 21 examples of isoindigos, only IId, 6BIId, and 66DBIId exhibit less well-defined shapes for the second redox wave. This is probably due to the rotational isomerisation of the one-electron reduced isoindigo radical anions. As shown in Supplementary Fig. 10, the C=C bond connecting the two oxindole rings becomes a single bond in the radical anion, allowing free rotation of the two rings. This creates rotational isomers and gives rise to shoulder peaks in the second redox process. Adding strong EWGs or substitution groups at the 5-position of isoindigo can create dipole-dipole repulsion or steric hindrance, inhibiting rotational isomerisation and resulting in a more reversible second redox process. Similarly, adding CO₂ onto isoindigos also creates dipole and steric hindrance, impeding the rotational isomerisation and leading to more defined CV curves.

Ideal EMCC sorbents shall have redox potentials more positive than the oxygen reduction potential (−1.35 V vs. Fc⁺/Fc in DMF, Supplementary Fig. 11) to minimise sorbent sensitivity towards O₂. With stronger or increasing numbers of EWG introduced to the isoindigo rings, the redox potential exhibits an increasing anodic shift in the

sequence of -F, -Br, -COOMe, -CONHR, and -NO₂ substituent groups from mono- to tetra-substitution (Fig. 5a and Supplementary Table 2). Through a close examination of the structure-property relationship, we hypothesise that the anodic shift is attributed to not only the commonly expected electronic state tuning from the EWG substituents but also the intramolecular hydrogen bonding effect (α shown in Fig. 4b and c). This is because hydrogen bonding can decrease the electron density of the redox-active oxygen centre to facilitate reduction. The downfield shift of proton at 4-position (H^a) in isoindigos with EWG substituents suggests the formation of stronger hydrogen bonding (α) (Table 1 and Supplementary Table 2).

To verify the above hypothesis, we show that EWG substituent at 5-position is more effective in facilitating electro-reduction than that at 6-position. This is because the former is in the ortho-position of H^a and more effective in pulling away the electron density, thereby inducing a stronger hydrogen bonding (Fig. 4d). For instance, 55DBIId and 66DBIId exhibit very close ¹H NMR peaks for H^a (11.11 and 11.10 ppm, Supplementary Fig. 12), suggesting similar degrees of electron deficiency in these two molecules. In contrast, the chemical shift of H^a is 9.32 and 8.99 ppm for 55DBIId and 66DBIId, respectively, clearly indicating a stronger hydrogen bonding (α) in the 5-substituted species. Therefore, $E_{1/2}(\text{IId}/\text{IId}^{\bullet-})$ of 55DBIId (−1.09 V vs. Fc⁺/Fc) is more positive compared to 66DBIId (−1.12 V vs. Fc⁺/Fc). This trend is consistent for all examples in our isoindigo family (Supplementary Table 2, e.g., 5BIId vs. 6BIId and 6MCIId vs. 5NIId vs. 5N6MCIId) and is further confirmed with DFT calculations (details *vide post*).

Counterintuitively, adding electron-donating groups (EDGs) such as methoxy shows a negligible influence on $E_{1/2}(\text{IId}/\text{IId}^{\bullet-})$, as evidenced by IId vs. 55DMIId (both show $E_{1/2}$ of −1.29 V vs. Fc⁺/Fc, Table 1), and 5NIId vs. 5M5NIId (both show $E_{1/2}$ of −1.08 V vs. Fc⁺/Fc, Supplementary Table 2). This is likely due to the charge-transfer effect that lowers the energy level of the molecule, offsetting the electronic effect from EDGs. Specifically, isoindigo species are electron acceptors (n-type organic semiconductors)²⁸, where charge transfer can be induced between the electron-deficient isoindigo rings and the electron-rich methoxy group. UV-vis absorption spectra suggest an optical bandgap of 1.90–1.98 eV for most isoindigos with or without chemical modification (Supplementary Table 2 and Supplementary Figs. 13–15). However, the bandgaps drop to 1.78 and 1.71 eV for methoxy substituted 55DMIId and 5M5NIId, manifesting charge transfer in these two compounds.

Breaking the scaling relationship between redox potential and CO₂ affinity

After understanding the effect of molecular structures on the redox potentials of isoindigos, we further study their CO₂ binding behaviours. All isoindigos in this work exhibit anodically shifted potential for the second electron transfer process under CO₂, confirming their ability to form CO₂ adducts upon electro-reduction. Importantly, through the combined effect of EWGs substitution and hydrogen bonding (α) discussed above, all isoindigos with unsubstituted H^a display $E_{1/2}$ values anodic to oxygen reduction under CO₂, implying favourable stability of isoindigo sorbents against O₂.

In all previous reports on redox-tunable CO₂ sorbents, anodically shifted redox potential always comes with significantly diminished CO₂ binding affinity (Supplementary Table 1). However, another key finding of this work is that hydrogen atom (H^b) on the lactam-N of isoindigos can induce intermolecular hydrogen bonding with the complexed CO₂ molecule to thermodynamically stabilise the CO₂ adduct (Fig. 4e). As a result, regardless of $E_{1/2}$, the log K_{CO_2} values of isoindigos with unsubstituted H^b were found to be relatively constant (Table 1 and Supplementary Table 2, see Supplementary Note 3 for details on K_{CO_2} calculation), suggesting the high tolerance of such redox carriers to a wide range of chemical modifications.

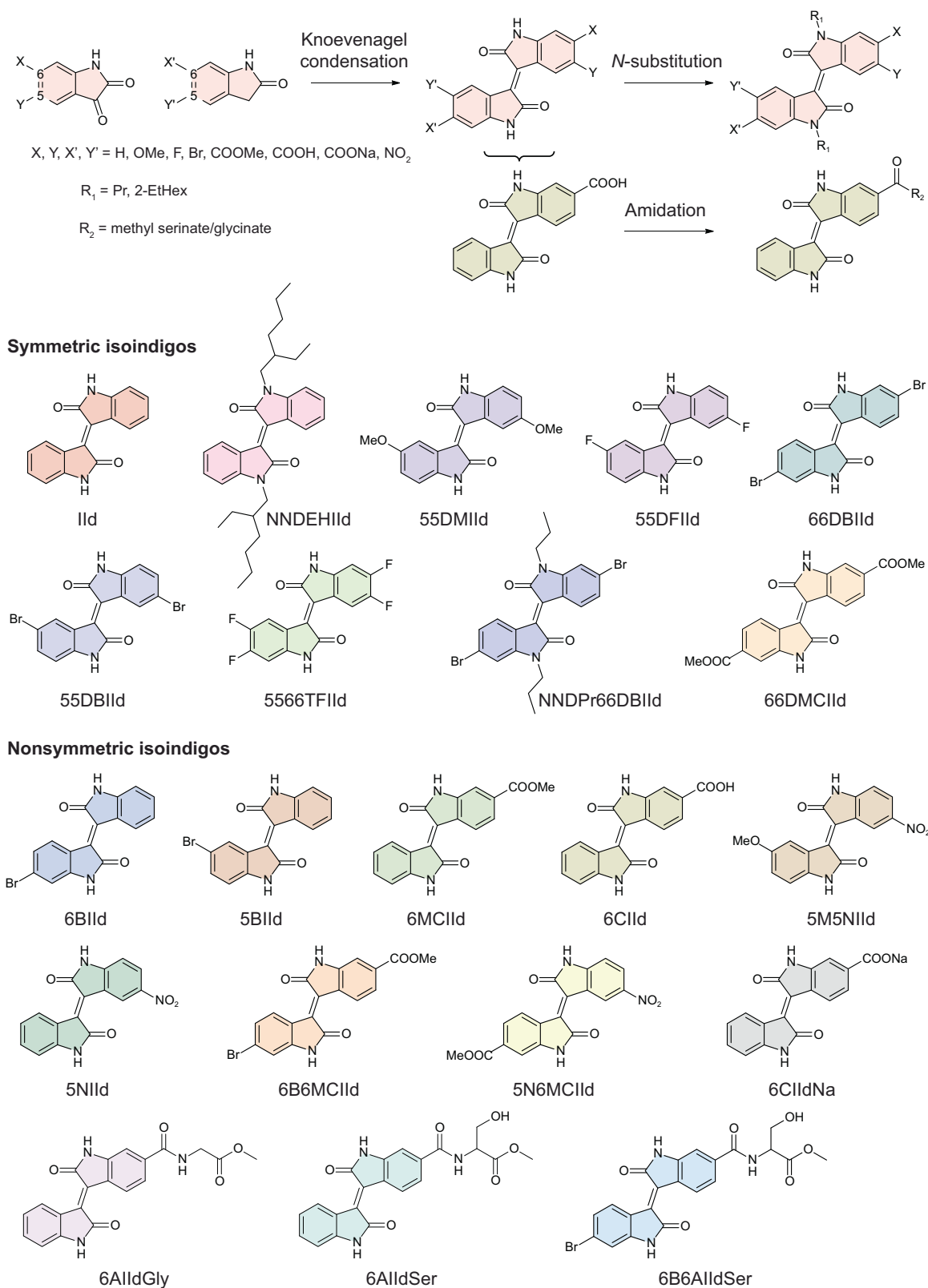


Fig. 3 | Modular synthesis of redox-tunable isoindigo sorbents for EMCC. Functional groups can be pre-installed onto the precursors of isoindigos and various isoindigos can be obtained through Knoevenagel condensation of the

precursors. Amino acid ester can be further installed through amidation reaction with carboxylic acid modified isoindigos.

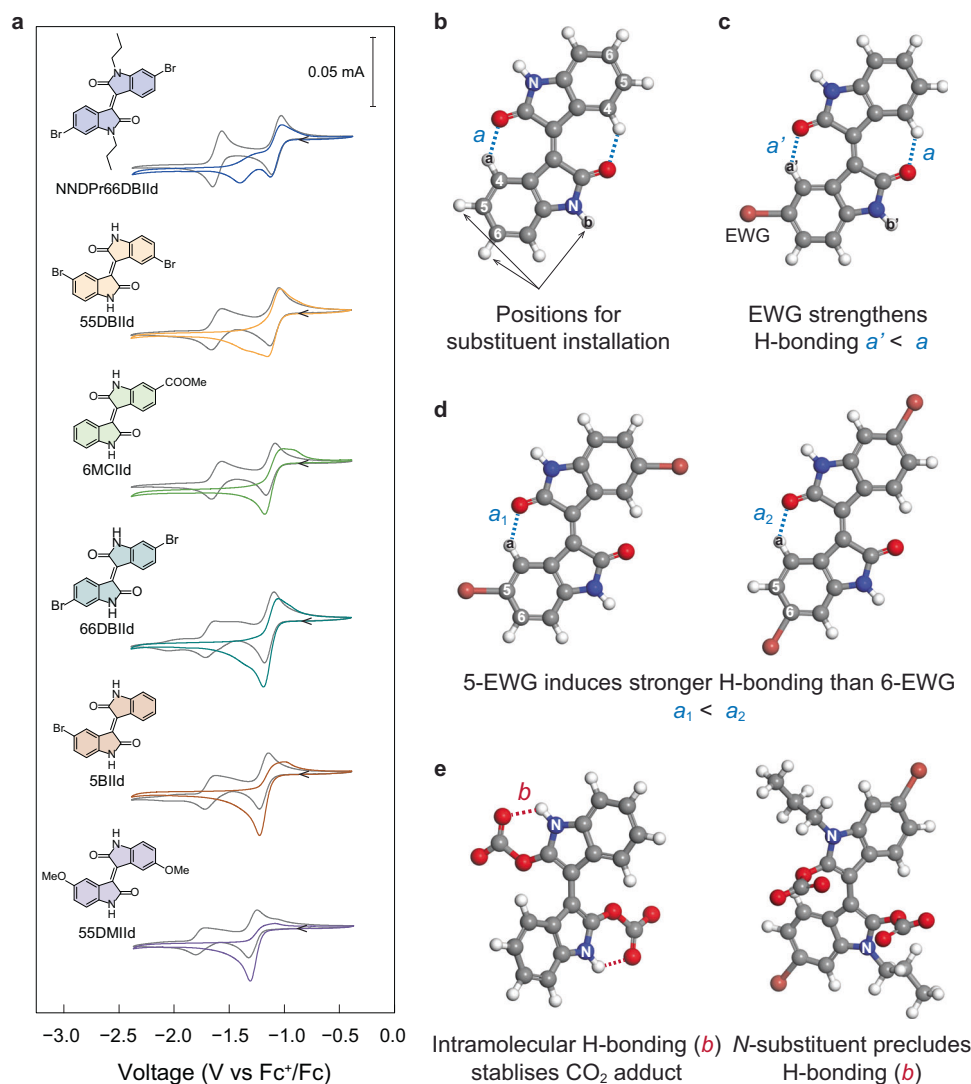


Fig. 4 | Structure-property relationships of redox-tunable isoindigo-based CO₂ sorbents. **a** CV of various isoindigos using 2.5 mM compound in DMF with 0.1 M NBu₄PF₆ under N₂ (grey) or CO₂ (coloured). The CV curves were recorded at a scan rate of -50 mV s^{-1} at 298 K. **b** DFT-optimized structure of IId; positions for introducing substituent groups are labelled, which are at 5, 6, and lactam *N*-position; intramolecular hydrogen bonding (**a** indicates bond length) in the neutral state is shown as blue dashed lines. **c** DFT-optimized structure of 5BIId suggests EWG can

strengthen the hydrogen bonding (**a**). **d** DFT-optimized structures of 55BIId (left) and 66DBIId (right) showing that EWG substituent at 5-position is more effective in strengthening the hydrogen bonding (**a**). **e** DFT simulation showing that intramolecular hydrogen bonding (**b**) indicates bond length, red dashed lines) occurs in the CO₂ adduct, stabilising the CO₂ binding. Colour of atoms: grey: C; red: O; blue: N; brown: Br; white: H.

To further demonstrate the role of hydrogen bonding (**b**) on CO₂ adduct stabilisation, we synthesised two examples with *N*-substitutions to eliminate this hydrogen bonding (NNPr66DBIId and NNDEHIId). Compared with 6,6'-dibromo substituted 66DBIId ($\log K_{\text{CO}_2} = 9.59$), the CO₂ binding constant of *N*-alkylated NNPr66DBIId ($\log K_{\text{CO}_2} = 4.48$) shows a dramatic decrease of five orders of magnitude (Table 1). A similar phenomenon was observed between NNDEHIId ($\log K_{\text{CO}_2} = 6.62$, Supplementary Table 2) and IId ($\log K_{\text{CO}_2} = 9.34$). Besides, we designed an isoindigo bearing a carboxylic acid group (6MCIId), which serves as a free proton donor to disrupt the intramolecular hydrogen bonding (**b**). As a result, the CO₂ binding ability of reduced 6MCIId almost diminished with a low $\log K_{\text{CO}_2}$ of 2.87 (Supplementary Table 2).

To visualise our success in breaking the scaling relationship between redox potential and CO₂ binding affinity, we plot the change in K_{CO_2} relative to unmodified IId against $E_{1/2}$ of the first electron transfer under N₂ (Fig. 5b). Upon installing EWGs, $E_{1/2}$ can be effectively shifted from -1.29 V to -0.97 V vs. Fc⁺/Fc. Nevertheless, the K_{CO_2} values

exhibit minimal changes within only one order of magnitude, as long as the lactam-N is unsubstituted to facilitate intramolecular hydrogen bonding. Furthermore, linear fitting shows a negligible correlation ($R^2 < 0.1$), underlining that our molecular design strategy can indeed break the scaling relationship between redox potential and CO₂ binding affinity.

We further tested the bimolecular rate constant ($k_{\text{bimolecular}}$) for the reaction between isoindigo radical anion and CO₂ (Supplementary Figs. 16–19, Supplementary Table 3, see Supplementary Note 3 for details in measurement). With intramolecular hydrogen bonding (**b**) in the CO₂ adduct, 6MCIId, 6AIIdSer, and 66DBIId display a similar rate constant of $22.5\text{--}18.6 \text{ M}^{-1} \text{ s}^{-1}$. However, the *N,N*-disubstituted NNPr66DBIId exhibits a decreased rate constant of $3.3 \text{ M}^{-1} \text{ s}^{-1}$, manifesting that intramolecular hydrogen bonding (**b**) is also conducive to CO₂ complexation kinetics.

At a CO₂ concentration of 20% or 10%, the CV curves of isoindigos usually exhibit a positively shifted second reduction peak compared to that under N₂; however, most do not completely

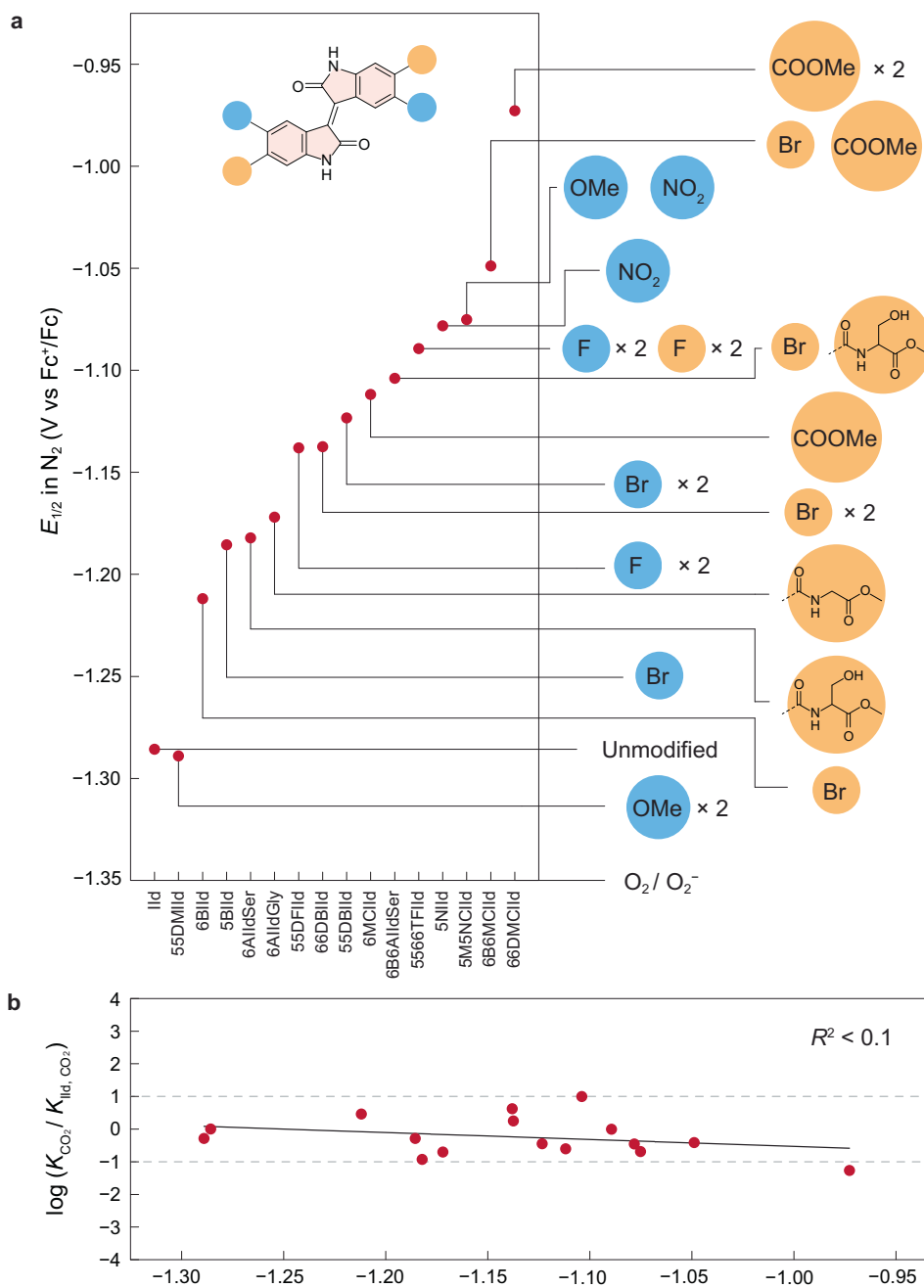


Fig. 5 | The substituent effect on the redox potentials and CO₂ binding abilities of isoindigos. **a** The effect of substituent group on the first electron-transfer half-wave potentials under N₂. **b** The plot between the first electron transfer half-wave

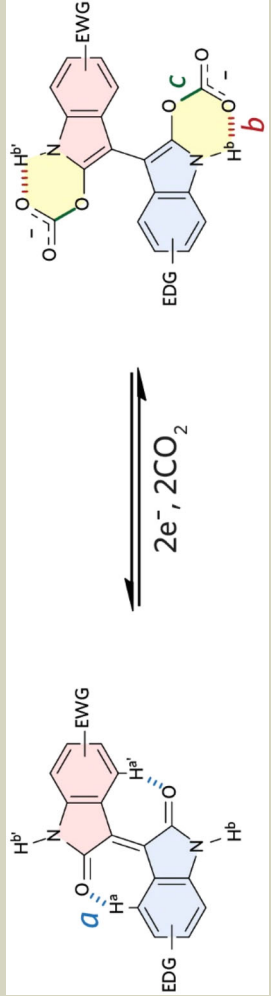
potential under N₂ and the change in CO₂ binding constant relative to unmodified isoindigo. There is no linear correlation ($R^2 < 0.1$) between the relative CO₂ binding constants and the half-wave potentials.

emerge into the first (Supplementary Fig. 7 and 8). The phenomenon is attributed to the kinetic competition between the chemical transformation of IId^- into $[\text{IId-CO}_2]^-$ ($r = k_{\text{bimolecular}}[\text{CO}_2][\text{IId}^-]^{29}$, where $[\text{CO}_2]$ and $[\text{IId}^-]$ are the concentrations of CO₂ and IId^-) and the electrochemical reduction of $[\text{IId-CO}_2]^-$. Higher CO₂ concentrations lead to higher r , which facilitates the formation of $[\text{IId-CO}_2]^-$ and ultimately leads to a single, merged reduction peak. Correspondingly, we tested the CV of 6MCIId at different scan rates and indeed observed the gradual merging of the two reduction peaks with slower scans (Supplementary Fig. 20). Therefore, the separation between the two cathodic peaks under low CO₂ concentrations can serve as a qualitative indicator for CO₂ complexation kinetics.

As a final note, CO₂ complexation can be frustrated when introducing highly strong EWGs or strong hydrogen bonding acceptors to isoindigo (5N6MCIId and 6CIIdNa). Detailed analysis is included in Supplementary Note 4 and Supplementary Fig. 21.

Detailed investigation on the role of hydrogen bonding

Distinct from previously reported redox-tunable CO₂ carriers, isoindigos possess intramolecular hydrogen bondings in both inactivated (neutral) and activated (reduced) forms, accounting for their unique EMCC properties. Therefore, we selected the seven most representative structures from our library and carefully compared various parameters such as NMR spectra, density functional theory (DFT)-optimised bond lengths, redox potentials, and CO₂ binding constants

Table 1 | The interplay between substituent groups and intramolecular hydrogen bondings in isoindigos and the corresponding impacts on redox potentials (V vs. Fc⁺/Fc) and CO₂ binding


Isoindigos	¹ H NMR (H ^a) (ppm) ^a	¹ H NMR (H ^b) (ppm) ^a	Bond length of a (Å) ^b	Bond length of b (Å) ^b	Bond length of c (Å) ^b	E _{1/2} (IId/IId ^{•-}) in N ₂ (V vs Fc ⁺ /Fc)	log K _{CO₂}
IId	9.06	10.89	1.963	1.954	1.461	-1.29	9.34
55DMIId	8.85	10.69	1.953	1.97	1.463	-1.29	9.05
5BIId	9.07	10.96	1.962	1.957	1.463	-1.19	9.05
5BIId (EWG)	9.31	11.05	1.936	1.943	1.467	-1.19	9.05
55DBIId	9.32	11.11	1.939	1.946	1.469	-1.09	9.33
6MCIId	9.07	10.94	1.960	1.954	1.954	-1.12	8.89
6MCIId (EWG)	9.15	11.08	1.956	1.944	1.476	-1.12	8.89
66DBIId	8.99	11.1	1.961	1.942	1.468	-1.14	9.59
NNDP-r66DBIId	9.05	NA	1.948	NA	1.486	-1.07	4.87

^a ¹H NMR were recorded on the neutral molecules in DMSO-d₆ using solvent residual peak as the internal reference for calibration. ^b Bond length was obtained from DFT-optimised structures. ^c Results from the non-symmetric oxindole ring with the EWG-substituent.

to investigate the interplay between substituent groups and hydrogen bonding on the thermodynamic properties of isoindigos. Key data are summarised in Table 1 (also see Supplementary Figs. 22 and 23 for DFT-optimised structures). DFT calculation shows that the theoretical first electron transfer potential shifts anodically in the order of IId, 5BIId, 66DBIId, and 55DBIId, consistent with experimental observation (Supplementary Table 4). Besides, DFT-calculated CO₂ binding constants ($\log K_{\text{CO}_2}$) of the isoindigos agree well with the trend of our experimental results (Supplementary Table 5). DFT-optimised structures further confirm the formation of intramolecular hydrogen bonding (**a**) and (**b**).

The electron density of H^a at 4-position and H^b at *N*-position can be regarded as indicators of the bond strength of **a** and **b**, respectively. Specifically, ¹H NMR spectra reveal a chemical shift of 9.06 ppm for H^a and 10.89 ppm for H^b in unmodified IId, corresponding to a DFT-optimised bond length of 1.963 Å for **a** and 1.954 Å for **b**. Introducing electron-withdrawing bromo groups at 5-position (55DBIId) downfield shifts H^a to 9.32 ppm and H^b to 11.11 ppm, resulting in an enhanced hydrogen bonding of 1.939 Å for **a** and 1.946 Å for **b**, respectively. Interestingly, the electronics and hydrogen bonding of each oxindole ring can be independently tuned in nonsymmetric isoindigos. Using the nonsymmetric 5BIId as an example, the chemical shifts of H^a and H^b are 9.07 and 10.96 ppm at the non-substituted side, corresponding to a DFT-optimised bond length of 1.962 Å for **a** and 1.957 Å for **b**, which is very close to IId. In contrast, H^a and H^b shift downfield to 9.31 and 11.05 ppm at the bromo-substituted side, corresponding to an enhanced hydrogen bonding of 1.936 Å for **a** and 1.943 Å for **b**.

Moreover, introducing the same EWG at different positions modulates the strength of hydrogen bonding (**a**) differently. For example, with the same dibromo-substitution, the chemical shift of H^a in 66DBIId (8.99 ppm) is upfield to that of 55DBIId (9.32 ppm). This results in a weakened hydrogen bonding (**a**) of 1.961 Å in 66DBIId than that of 1.939 Å in 55DBIId, explaining the more negative reduction potential of 66DBIId (−1.14 V vs. Fc^{+/}Fc) than 55DBIId (−1.09 V vs. Fc^{+/}Fc). The above results strongly suggest that, in addition to the electronic effect of substituent groups, intramolecular hydrogen bonding (**a**) is also vital in facilitating the reduction of isoindigo.

Although decreasing the electron density of isoindigos by introducing EWGs at 5,6-positions can effectively facilitate their reduction, counterintuitively, the reduced isoindigos exhibit negligible decay in CO₂ affinities, underscoring the importance of intramolecular hydrogen bonding (**b**). Using DFT calculation, we found that the nucleophilicity of the oxygen centre indeed weakens when EWG is introduced, as suggested by the increased length of the carbonate C–O bond (**c**). For instance, the bond length of **c** on the oxindole ring with –COOMe group is increased by 1.2 pm compared to that on the non-substituted ring in 6MCIId. However, as mentioned above, hydrogen bonding (**b**) strengthens with stronger or increasing number of EWG substituents to keep the bond length of **c** nearly constant. Moreover, the DFT-optimised structure suggests that hydrogen bonding (**b**) is precluded in NNDPr66DBIId, and the carbonate bends out-of-plane to the reduced isoindigo rings due to steric repulsion. Thus, the bond length of **c** in NNDPr66DBIId is increased by 1.8 pm compared to 66DBIId, giving rise to a significant drop in K_{CO_2} by almost five orders of magnitude.

The collective information above confirms our key conclusions. First, hydrogen bonding (**a**) can reduce the electron density at the redox centre and facilitate reduction. Second, hydrogen bonding (**a**) can be tuned by substituent groups, where EWG at 5-position is more effective than 6-position to shorten the bond length of **a** and hence facilitate reduction. Third, hydrogen bonding (**b**) stabilises the complexed CO₂ when EWGs are introduced.

It is important to note that the effect of intramolecular hydrogen bonding on CO₂ complexation has been briefly studied in prior works using quinones. However, it was observed that hydrogen bonding

occupies the CO₂ binding sites of quinones and diminishes the ability for CO₂ capture^{14,30}. Therefore, our work presents the first demonstration that intramolecular hydrogen bonding can facilitate CO₂ adduct formation and break the intrinsic linear free-energy relationship of EMCC chemistries. This is attributed to the unique chemical structure of isoindigo that allows free rotation of the oxindole rings in the reduced state as supported by DFT simulation, breaking the intramolecular hydrogen bonding (**a**) to create space for CO₂ complexation, which is further enhanced by the intramolecular hydrogen bonding (**b**) through the amide functionality.

Finetuning the properties of isoindigos

Breaking the correlation between chemical modification and CO₂ binding affinity greatly enhances the degree of freedom in finetuning sorbent properties. For instance, by installing EWGs such as methyl carboxylate, $E_{1/2}$ of 66DMCIId under CO₂ can be positively shifted by 300 mV compared to that of unmodified IId to impart O₂ stability, while the $\log K_{\text{CO}_2}$ only drops slightly (from 9.34 to 8.07). Besides, 66DMCIId is almost insoluble in organic solvents such as DMF (solubility < 2.5 mM), suggesting its potential as absorbent electrodes in fixed-bed EMCC devices.

Unmodified IId has a moderate solubility in DMF (~230 mM), which needs to be improved for practical use in flow-based EMCC systems⁷. To facilitate chemical functionalisation, we introduced a carboxyl group to the 6-position of isoindigos, which can be easily connected with amino acids through amidation reactions. As a proof of concept, we utilised glycine methyl ester and serine methyl ester as solubility enhancers and three nonsymmetric isoindigos were prepared (6AIIdGly, 6AIIdSer, and 6B6AIIdSer). 6B6AIIdSer features halogen substitution on one oxindole ring to tune redox potentials and amino acid ester functionalisation on the other oxindole ring to enhance solubility. To our delight, the solubilities of 6AIIdGly, 6AIIdSer, and 6B6AIIdSer increase to 606, 830, and 568 mM in DMF, respectively (Supplementary Table 6), likely due to the enhanced molecular interaction between the polar functional groups (amide and carboxylate) and DMF solvent. This is supported by the fact that 6AIIdSer is more soluble than 6AIIdGly due to the additional hydroxyl group from the serine moiety.

Conventional amine scrubbing sorbents have raised environmental concerns due to their biotoxicity^{31,32}. Here, we show that introducing amino ester functionalities into isoindigos substantially improves their biocompatibility with mammalian cells. Unmodified IId shows a LC₅₀ (lethal concentration that causes 50% cell death) of 11.2, 50.4, and 15.8 µg ml^{−1} for NIH3T3/GFP mouse fibroblasts, U2OS.EGFP human osteosarcoma cells, and MCF10A human breast epithelial cells, respectively, after 48 h cell culture (Supplementary Fig. 24 and 25). In comparison, the serinate-modified counterpart does not display clear toxicity under concentrations up to 100 µg ml^{−1} for NIH3T3/GFP and U2OS.EGFP, and has a significantly improved LC₅₀ of 89.4 µg ml^{−1} for MCF10A.

Effects of electrolytes, oxygen, and water

Before evaluating the CO₂ capture performance of isoindigos in EMCC devices, we assessed the influence of electrolytes and common gas stream impurities such as water and O₂ on their CO₂ binding properties. Using 55DBIId as an example, the electrochemical behaviours remained almost unaffected up to a high O₂ content (16% CO₂ and 20% O₂, Supplementary Fig. 26). Under N₂, the CV curves of 55DBIId remain reversible even at a high water content of 10 vol% (Supplementary Fig. 27). The declining peak current is caused by the decreasing isoindigo solubility with increasing water content. However, the expected CO₂ release at approximately −1 V vs. Fc^{+/}Fc gets suppressed in the presence of 10 vol% water, possibly due to the involvement of pH-swung process under high water content that requires higher energy input for CO₂ release.

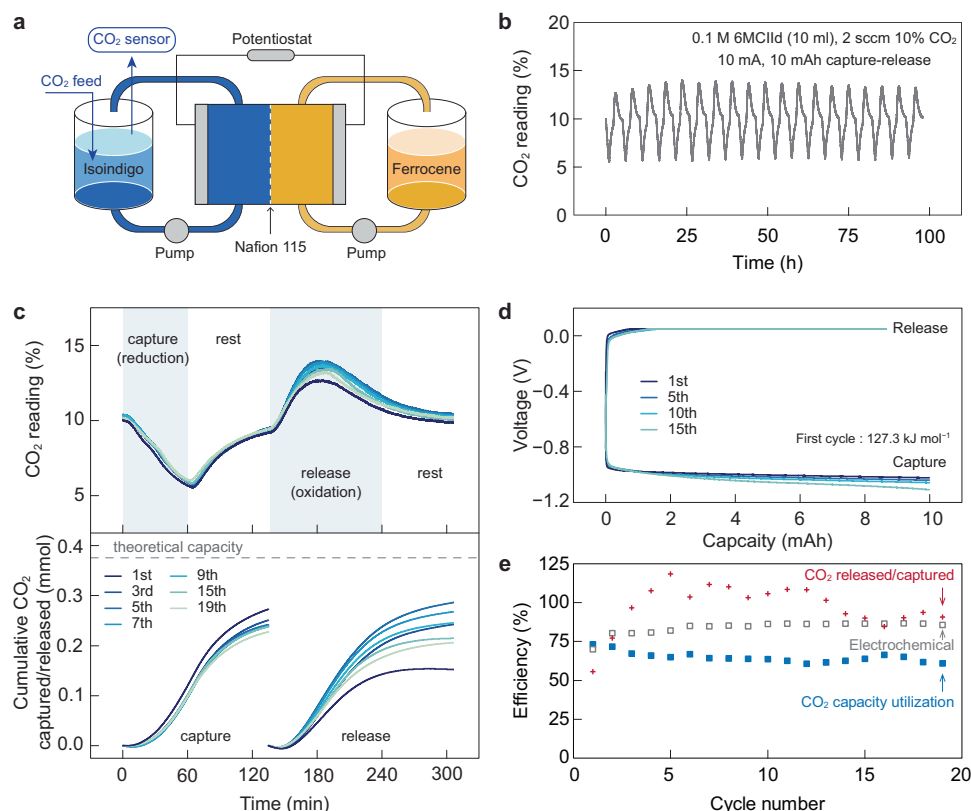


Fig. 6 | Evaluating the performance of 6MClId in the flow-based EMCC prototype. **a** Schematic of the flow-based EMCC prototype. **b** CO₂ reading at the exit of the sorbent tank over 19 repeating capture/release cycles for ~100 h of operation. **c**, The CO₂ reading of selected capture/release cycles overlaid, with the cumulative amount of CO₂ captured/released in each cycle relative to the theoretical capacity. Lighter colours represent later cycles. The shaded regions indicate the capture, rest, release, and rest steps. For CO₂ capture, 6MClId was reduced at 10 mA for 60 min followed by a 75 min rest. For CO₂ release, the adducts were oxidised at 10 mA to 0.05 mV followed by a 120 min constant voltage hold, and finally rested for another 75 min. **d** Selected voltage-capacity curves for the 1st, 5th, 10th, and 15th

capture/release cycle. **e** The CO₂ capacity utilisation efficiency (blue squares), release/capture efficiency (red crosses), and electrochemical efficiency (empty grey squares) of the system. The liquid sorbent was composed of 10 ml 0.1 M 6MClId in DMF with 0.25 M NaClO₄ as the supporting salt. The sorbent tank was filled with plastic beads and purged with 10% CO₂ at a flow rate of 2 standard cubic centimetres per minute (sccm). On the opposite side, a Fc tank was used to balance the charge, which was filled with 20 ml 0.1 M Fc in DMF with 0.25 M NaClO₄ as the supporting salt, 4 mM ferrocenium tetrafluoroborate (FcBF₄) to facilitate Fc oxidation, and 10 mM 6MClId to mitigate sorbent crossover.

We also studied the influence of supporting salt on the redox and CO₂ binding behaviours of isoindigos (Supplementary Fig. 28). The most prominent effect comes from the choice of cation, where reducing the size of cation leads to anodically shifted reduction potential, as is explained by the electrostatic interaction between cation and reduced isoindigo. Smaller alkaline cations exhibit stronger Lewis acidity, allowing tighter binding with reduced isoindigo to facilitate electro-reduction. Therefore, a more acidic supporting salt cation can further enhance the robustness of isoindigo against O₂. Nevertheless, it may also slow down the CO₂ complexation kinetics due to the competition between cation and CO₂ for binding with reduced isoindigo.

Evaluating the isoindigo sorbents in flow-based EMCC prototypes

Based on the CV peak potentials for CO₂ capture and release, we estimated the theoretical minimum energy requirement for CO₂ separation using isoindigo sorbents, which ranges from 9.8 to 27.6 kJ mol⁻¹ CO₂ (Supplementary Fig. 29). It is noteworthy that these molecules show very close onset potentials for CO₂ capture and release such that the theoretical energetics calculated from CV peak potentials can be overestimated compared to previous calculations using onset values¹⁷. As a proof of concept, we evaluated their intrinsic capability for reversible CO₂ capture and release in a flow-based EMCC prototype reported by us previously (Fig. 6a)¹⁷. Detailed testing conditions are provided in the Supplementary Information.

Figure 6b shows the cyclic capture-release performance of 6MClId using 10% CO₂ (balanced by N₂) as the gas feed. The CO₂ reading curves of each cycle are overlaid in Fig. 6c, where the cumulative CO₂ captured/released is obtained by integrating these curves. For each cycle, 6MClId was reduced at 10 mA for 60 min, and the decrease in CO₂ concentration at the gas outlet confirmed carbon capture. The current was then stopped for 75 min, allowing the CO₂ reading to gradually return to the baseline as the reduced isoindigo fully reacted with CO₂. The CO₂ adduct was subsequently oxidised following a constant current-constant voltage (CC-CV) protocol, and the continuous increase in CO₂ concentration above 10% indicated CO₂ desorption. Afterward, the current was set to zero again to ensure the complete release of the oversaturated CO₂ from the sorbent electrolyte. The oxidation-reduction profiles of the flow system are shown in Fig. 6d. By integrating the voltage-capacity curves, the electrical energy consumption under 10% CO₂ is estimated as 127.3 kJ mol⁻¹ CO₂ in the first cycle and 142.5 ± 8.2 kJ mol⁻¹ CO₂ over the first 16 cycles (Supplementary Fig. 30), which is comparable to other carbon capture technologies^{18–20,33–38}.

Figure 6e summarises the three key metrics commonly used for evaluating EMCC performance. CO₂ capacity utilisation, defined as the amount of CO₂ captured relative to the theoretical value (one CO₂ per electron), shows an average of 65% over 19 cycles, which is competitive against the state-of-the-art quinone-based sorbent reported recently¹⁹. The release/capture efficiency, defined as the ratio of the total amount

of CO₂ released and captured in each cycle, is averaged to be 97%, indicating the good reversibility of the sorbent. Considering a relatively constant electrochemical (Coulombic) efficiency of the EMCC prototype at -84%, the major loss should be attributed to two factors: (1) our CC-CV protocol where the CO₂ adduct was not fully oxidised; (2) the crossover of sorbents and counter electrolytes caused by membrane swelling, which limits all current nonaqueous redox-flow electrochemical systems. 6MCIId was also evaluated at a higher percentage of CO₂ removal (Supplementary Fig. 31).

In addition to 6MCIId, we evaluated the performance of other isoindigo sorbents such as 55DBIId (Supplementary Fig. 32), 66DBIId (Supplementary Fig. 33), and 6B6AIIIdSer (Supplementary Fig. 34). 55DBIId achieved an average CO₂ utilisation efficiency of up to -80% and an average release/capture efficiency of -80%. Using 66DBIId, we studied ¹H NMR of the crude sorbent electrolyte after 11 capture/release cycles over 50+ hours (Supplementary Fig. 35). The spectrum suggests the high stability of 66DBIId after cycling and also the severe crossover issue of the ferrocene counter electrolyte (three times the concentration of 66DBIId in the sorbent tank), which explains the decay in electrochemical capacity of current EMCC prototypes. Besides, we can recover 66DBIId with 87% yield from the sorbent electrolyte after cycling, corroborating the robustness of the sorbent. In addition, we found -24% of 66DBIId isomerised into *cis*-66DBIId, supporting our hypothesis on the rotational isomerisation of reduced 66DBIId discussed earlier (Supplementary Fig. 10). Nevertheless, the reduction of both 66DBIId and its *cis*-isomer yield the same activated CO₂ sorbent, which we believe does not affect the long-term stability of the EMCC prototype.

To our delight, 6B6AIIIdSer exhibits a much lower oxidation potential for CO₂ release, likely due to its higher solubility. Moreover, 6B6AIIIdSer shows excellent cycling stability with negligible voltage decay over >40 cycles and -200 h of operation with a capacity degradation rate of 2% (Supplementary Note 5).

We further tested the EMCC performance of 6MCIId using simulated flue gas (10% CO₂ + 3% O₂ balanced in N₂) (Supplementary Fig. 36). The cell can run stably over -90 h with reduction voltage maintained above -1.3 V, which minimised the parasitic oxygen reduction reaction. A CO₂ capacity utilisation efficiency of -50% was achieved with a near unity CO₂ release/capture efficiency.

Finally, we evaluated the CO₂ capture capability of 6MCIId under low CO₂ concentration and its CO₂ release capability under pure CO₂. Using 1% CO₂ with 0.3% O₂ as the feed, we observe an early-stage energy consumption of 224.2 kJ mol⁻¹ CO₂ and a single pass CO₂ removal of >90% (Supplementary Fig. 37). This suggests that our intramolecular hydrogen bonding strategy is effective in improving CO₂ affinity for low-concentration CO₂ capture. In another experiment, the CO₂ capture-release behaviour under 100% CO₂ headspace was quantified using mass flow metre (Supplementary Fig. 38). Under conditions similar to low-concentration CO₂ capture, we show an early-stage energy consumption of 143.7 kJ mol⁻¹ CO₂ captured and 13.6 kJ mol⁻¹ CO₂ released, respectively.

In this study, we focus on exploring the fundamental chemistry of isoindigos as redox-active CO₂ carriers and their potential to overcome the linear free-energy relationship that limits the structural modification of EMCC sorbents. The flow-based prototype in this work is, however, not an ultimate design for practical systems but a proof-of-concept demonstration to evaluate the performance of isoindigo at the lab scale. We believe future efforts can substantially improve the performance by optimising the electrolytes, electrodes, and membranes of EMCC devices.

Comparison of methods for estimating CO₂ binding constants

As a final note, in this manuscript, we estimated the K_{CO_2} of isoindigos using the prevalent method adopted for quinones, bipyridines, and benzyl thiolate^{12,21,22}, providing an equitable comparison with

previously reported redox-active CO₂ carriers. Accordingly, we assume that the two-electron-reduced isoindigo binds to one molecule of CO₂ and calculate the K_{CO_2} based on $\Delta E_{\text{peak}}(2)$ under pure N₂ and CO₂ atmosphere, respectively (Supplementary Note 3). This method, therefore, eliminates the kinetic effects in CV under lower CO₂ concentrations. Alternatively, we recorded the CV of IId and 6MCIId under various CO₂ concentrations (Supplementary Fig. 39) and fitted the relationship between $\Delta E_{\text{peak}}(2)$ and CO₂ concentration (Supplementary Fig. 40 and Supplementary Note 7). Similar K_{CO_2} values were obtained for IId and 6MCIId on the order of 10¹², further confirming the high tolerance of EWG in isoindigo structural motifs for strong CO₂ binding. However, the fitting quality was unsatisfactory, with low R^2 values and unreasonable number of binding sites. Therefore, we took the former method to calculate K_{CO_2} for all isoindigos reported in this work.

Discussion

In summary, we demonstrate the rational design of a class of bifunctional redox-tunable CO₂ carriers based on isoindigo and their derivatives. The unique intramolecular hydrogen bonding in isoindigo moieties enables a wide range of chemical modifications to facilitate electro-reduction, tune solubility, and preclude parasitic reactions without compromising their CO₂ binding ability. With coupled experimental and computational studies, we provide an in-depth analysis of the structure-function relationships of isoindigos as EMCC sorbents. Compared to existing EMCC sorbents, isoindigo compounds have the following advantages: 1) a nearly constant log K_{CO_2} of -9 with high tolerance to chemical modifications; 2) facile synthesis with the ease of encoding functionalities; 3) highly tunable redox potentials and solubilities; 4) improvable biocompatibility. In addition to flow-based EMCC, we envisage that isoindigos can also find applications as solid adsorbents in fixed-bed systems, due to their descent charge mobility and the abundant methods in synthesising and processing isoindigo-based polymers developed by the community of organic semiconductors. The work paves the way for engineering more reliable EMCC systems by breaking the fundamental barriers of the scaling relationship between redox potential and CO₂ binding strength when designing redox-tunable CO₂ sorbents.

Methods

Synthesis of 6MCIId

To a mixture of isatin (1.47 g, 10 mmol) and methyl 2-oxindole-6-carboxylate (1.91 g, 10 mmol) in acetic acid (50 ml) was added 37% HCl solution (0.5 ml). The mixture was heated at reflux for 1 day under Argon atmosphere. The mixture was cooled to room temperature, filtered, and washed with water, ethanol, and ethyl acetate. The solid was dried in the vacuum oven at 60 °C for 15 h to afford a dark red powder (2.93 g, 92%). ¹H NMR (400 MHz, DMSO) δ 11.08 (s, 1H), 10.94 (s, 1H), 9.15 (d, J = 8.4 Hz, 1H), 9.07 (d, J = 8.0 Hz, 1H), 7.57 (dd, J = 8.4, 1.7 Hz, 1H), 7.38 (td, J = 7.7, 1.2 Hz, 1H), 7.34 (d, J = 1.6 Hz, 1H), 7.02 – 6.94 (m, 1H), 6.85 (d, J = 7.3 Hz, 1H), 3.87 (s, 3H). ¹³C NMR (101 MHz, DMSO) δ 168.68, 168.62, 165.57, 144.70, 143.91, 135.73, 133.47, 131.95, 131.79, 129.83, 129.06, 125.68, 121.98, 121.51, 121.28, 109.69, 109.29, 52.29.

Electrochemical measurements

Electrochemical measurements were performed with a BioLogic VSP potentiostat from BioLogic Science Instruments. Cyclic voltammetry (CV) utilised a glassy carbon electrode (3 mm diameter) as the working electrode, a platinum wire as the counter electrode, and a silver wire as the quasi-reference electrode, with ferrocene as the internal reference. In a standard CV test, isoindigo (2.5 mM) was dissolved in anhydrous DMF with 100 mM NBu₄PF₆ as the supporting electrolyte. CV were typically recorded at a scanning rate of -50 mVs⁻¹ with a cut-off potential from -1.5 to 0.5 V (prior to ferrocene calibration). To examine the effects of ionic species on the redox behaviour of the sorbent

molecules, supporting electrolyte salts including 100 mM LiClO₄, NaClO₄, KClO₄, NBu₄ClO₄, sodium triflate (NaOTf), or sodium bis(trifluoromethanesulfonyl)imide (NaTFSI) was employed, respectively. The electrochemical data were gathered and analysed by EC-lab V11.50.

Flow-based EMCC prototype

In a standard setup, a scintillation vial (20 ml) with a septum cap, serving as the sorbent tank, was continuously purged with CO₂ feed gas (balanced with N₂) at a controlled flow rate using an Alicat mass flow controller. Simulated flue gas conditions were mimicked using a 10% CO₂ and 3% O₂ mix, balanced by N₂. CO₂ levels were continuously monitored at the gas outlet using an infra-red-based CO₂ sensor (SprintIR-W 100%), with data recorded via Labview 2021. To minimise mixing time in the overhead space, the tank was filled with plastic beads from McMaster-Carr. The Fc tank was maintained without air exposure. Sorbent and Fc electrolytes were circulated at a flow rate of 10 ml min⁻¹ through a commercial flow cell (Scribner) by a two-channel peristaltic pump (Masterflex). The flow cell incorporated two graphite plates with 5 cm² interdigitated flow fields, pressing against two pieces of carbon paper electrodes (Sigraet 28 AA) on each side of the graphite electrodes. A Nafion 115 membrane, flanked by polypropylene sheets, was placed between the carbon electrodes. The cell was sealed by Kalrez fluoropolymer elastomer gaskets (0.02-inch thick). CO₂ capture was conducted in constant current mode, while release followed a constant current/constant voltage protocol: the adduct was first oxidised at a constant current until reaching a cut-off voltage and then held at that voltage until the current value fell below 5% of the original constant current). For experiments using 5 cm² flow fields, the CO₂ capture-release was cycled at a current of 10 mA with a cut-off potential of 0.05 V in the release process. For experiments using 25 cm² flow fields, the CO₂ capture-release was conducted at a current of 50 mA with a cut-off potential of 0.3 V in the release process. The cycling protocols of each experiment are provided in the corresponding figure captions. For experiments using 6MClIId sorbent, we added 10 mM 6MClIId and 4 mM ferrocenium tetrafluoroborate (FcBF₄) into the CE tank to mitigate sorbent crossover and facilitate the reduction of the oxidised ferrocenium in the counter electrolyte, respectively. For less soluble 55DBIId and 66DBIId, the sorbent was dispersed in dimethylacetamide (DMAc) to form a slurry catholyte.

Reporting summary

Further information on research design is available in the Nature Portfolio Reporting Summary linked to this article.

Data availability

The data generated or analysed during this study are included in the manuscript and its Supplementary Information. The main data generated in this study are provided in the Supplementary Information/Source Data file. Data are also available from the corresponding author upon request. Source data are provided with this paper.

References

1. Mac Dowell, N., Fennell, P. S., Shah, N. & Maitland, G. C. The role of CO₂ capture and utilization in mitigating climate change. *Nat. Clim. Change* **7**, 243–249 (2017).
2. Deutz, S. & Bardow, A. Life-cycle assessment of an industrial direct air capture process based on temperature–vacuum swing adsorption. *Nat. Energy* **6**, 203–213 (2021).
3. Bui, M. et al. Carbon capture and storage (CCS): the way forward. *Energy Environ. Sci.* **11**, 1062–1176 (2018).
4. Chu, S. Carbon capture and sequestration. *Science* **325**, 1599–1599 (2009).
5. Sanz-Pérez, E. S., Murdock, C. R., Didas, S. A. & Jones, C. W. Direct capture of CO₂ from ambient air. *Chem. Rev.* **116**, 11840–11876 (2016).
6. Sharifian, R., Wagterveld, R. M., Digdaya, I. A., Xiang, C. & Vermaas, D. A. Electrochemical carbon dioxide capture to close the carbon cycle. *Energy Environ. Sci.* **14**, 781–814 (2021).
7. Liu, Y., Lucas, É., Sullivan, I., Li, X. & Xiang, C. Challenges and opportunities in continuous flow processes for electrochemically mediated carbon capture. *iScience* **25**, 105153 (2022).
8. Rheinhardt, J. H., Singh, P., Tarakeshwar, P. & Buttry, D. A. Electrochemical capture and release of carbon dioxide. *ACS Energy Lett.* **2**, 454–461 (2017).
9. Renfrew, S. E., Starr, D. E. & Strasser, P. Electrochemical approaches toward CO₂ capture and concentration. *ACS Catal.* **10**, 13058–13074 (2020).
10. Barlow, J. M. et al. Molecular design of redox carriers for electrochemical CO₂ capture and concentration. *Chem. Soc. Rev.* **51**, 8415–8433 (2022).
11. Diederichsen, K. M. et al. Electrochemical methods for carbon dioxide separations. *Nat. Rev. Methods Prim.* **2**, 68 (2022).
12. Bell, W. L., Miedaner, A., Smart, J. C., DuBois, D. L. & Verostko, C. E. Synthesis and evaluation of electroactive CO₂ carriers. *SAE Trans.* **97**, 544–552 (1988).
13. Mizen, M. B. & Wrighton, M. S. Reductive addition of CO₂ to 9,10-phenanthrenequinone. *J. Electrochem. Soc.* **136**, 941–946 (1989).
14. Nagaoka, T., Nishii, N., Fujii, K. & Ogura, K. Mechanisms of reductive addition of CO₂ to quinones in acetonitrile. *J. Electroanal. Chem.* **322**, 383–389 (1992).
15. Rahimi, M., Khurram, A., Hatton, T. A. & Gallant, B. Electrochemical carbon capture processes for mitigation of CO₂ emissions. *Chem. Soc. Rev.* **51**, 8676–8695 (2022).
16. Scovazzo, P., Poshusta, J., DuBois, D., Koval, C. & Noble, R. Electrochemical separation and concentration of <1% carbon dioxide from nitrogen. *J. Electrochem. Soc.* **150**, D91 (2003).
17. Gurkan, B., Simeon, F. & Hatton, T. A. Quinone reduction in ionic liquids for electrochemical CO₂ separation. *ACS Sustain. Chem. Eng.* **3**, 1394–1405 (2015).
18. Voskian, S. & Hatton, T. A. Faradaic electro-swing reactive adsorption for CO₂ capture. *Energy Environ. Sci.* **12**, 3530–3547 (2019).
19. Diederichsen, K. M., Liu, Y., Ozbek, N., Seo, H. & Hatton, T. A. Toward solvent-free continuous-flow electrochemically mediated carbon capture with high-concentration liquid quinone chemistry. *Joule* **6**, 221–239 (2021).
20. Li, X., Zhao, X., Liu, Y., Hatton, T. A. & Liu, Y. Redox-tunable Lewis bases for electrochemical carbon dioxide capture. *Nat. Energy* **7**, 1065–1075 (2022).
21. Simeon, F. et al. Electrochemical and molecular assessment of quinones as CO₂-binding redox molecules for carbon capture. *J. Phys. Chem. C.* **126**, 1389–1399 (2022).
22. Barlow, J. M. & Yang, J. Y. Oxygen-stable electrochemical CO₂ capture and concentration with quinones using alcohol additives. *J. Am. Chem. Soc.* **144**, 14161–14169 (2022).
23. Bui, A. T., Hartley, N. A., Thom, A. J. W. & Forse, A. C. Trade-off between redox potential and the strength of electrochemical CO₂ capture in quinones. *J. Phys. Chem. C.* **126**, 14163–14172 (2022).
24. Hansch, C., Leo, A. & Taft, R. W. A survey of hammett substituent constants and resonance and field parameters. *Chem. Rev.* **91**, 165–195 (1991).
25. Wang, E., Mammo, W. & Andersson, M. R. 25th anniversary article: isoindigo-based polymers and small molecules for bulk heterojunction solar cells and field effect transistors. *Adv. Mater.* **26**, 1801–1826 (2014).
26. Bogdanov, A. V. & Mironov, V. F. Recent advances in the application of isoindigo derivatives in materials chemistry. *Beilstein J. Org. Chem.* **17**, 1533–1564 (2021).

27. Kiss, F. L., Corbet, B. P., Simeth, N. A., Feringa, B. L. & Crespi, S. Predicting the substituent effects in the optical and electrochemical properties of *N,N'*-substituted isoindigos. *Photochem. Photobiol. Sci.* **20**, 927–938 (2021).
28. Wei, X., Zhang, W. & Yu, G. Semiconducting polymers based on isoindigo and its derivatives: synthetic tactics, structural modifications, and applications. *Adv. Funct. Mater.* **31**, 2010979 (2021).
29. Xu, Y. et al. Assessing the kinetics of quinone–CO₂ adduct formation for electrochemically mediated carbon capture. *ACS Sustain. Chem. Eng.* **11**, 11333–11341 (2023).
30. Schimanofsky, C. et al. Direct electrochemical CO₂ capture using substituted anthraquinones in homogeneous solutions: a joint experimental and theoretical study. *J. Phys. Chem. C* **126**, 14138–14154 (2022).
31. del Rio, B. et al. The biogenic amines putrescine and cadaverine show in vitro cytotoxicity at concentrations that can be found in foods. *Sci. Rep.* **9**, 120 (2019).
32. Rohr, A. C. et al. Potential toxicological effects of amines used for carbon capture and storage and their degradation products. *Energy Procedia* **37**, 759–768 (2013).
33. Eisaman, M. D. et al. CO₂ separation using bipolar membrane electrodialysis. *Energy Environ. Sci.* **4**, 1319–1328 (2011).
34. Wang, M. et al. Flue gas CO₂ capture via electrochemically mediated amine regeneration: System design and performance. *Appl. Energy* **255**, 113879 (2019).
35. Wang, M., Herzog, H. J. & Hatton, T. A. CO₂ capture using electrochemically mediated amine regeneration. *Ind. Eng. Chem. Res.* **59**, 7087–7096 (2020).
36. Jin, S., Wu, M., Gordon, R. G., Aziz, M. J. & Kwabi, D. G. pH swing cycle for CO₂ capture electrochemically driven through proton-coupled electron transfer. *Energy Environ. Sci.* **13**, 3706–3722 (2020).
37. Jin, S., Wu, M., Jing, Y., Gordon, R. G. & Aziz, M. J. Low energy carbon capture via electrochemically induced pH swing with electrochemical rebalancing. *Nat. Commun.* **13**, 2140 (2022).
38. Liu, Y., Ye, H.-Z., Diederichsen, K. M., Van Voorhis, T. & Hatton, T. A. Electrochemically mediated carbon dioxide separation with quinone chemistry in salt-concentrated aqueous media. *Nat. Commun.* **11**, 2278 (2020).

Acknowledgements

We acknowledge support from the Johns Hopkins University, the Scialog program sponsored jointly by Research Corporation for Science Advancement and the Alfred P. Sloan Foundation, with additional support from Climate Pathfinders Foundation (grant #28438 X.L.), and the David and Lucile Packard Foundation. X.Z. acknowledges FDCT of Macau SAR (grant#0024/2022/ITP).

Author contributions

X.L. and Ya.L. conceived of the project and designed the experiments. X.L. conducted the experiments and analysed the data. X.Z. performed the DFT simulations under the supervision of Yu.L. L.Z. helped with the CV experiments and solubility test. A.M. helped analyse the carbon capture results. Y.X. performed the reaction rate tests and analysed the data. Z.F. conducted the biocompatibility tests under the supervision of L.G. Ya.L. supervised the whole project. X.L. and Ya.L. co-wrote the manuscript. All authors discussed the results and revised or commented on the manuscript.

Competing interests

The authors declare no competing interests.

Additional information

Supplementary information The online version contains supplementary material available at <https://doi.org/10.1038/s41467-024-45410-z>.

Correspondence and requests for materials should be addressed to Yayuan Liu.

Peer review information *Nature Communications* thanks the anonymous reviewers for their contribution to the peer review of this work. A peer review file is available.

Reprints and permissions information is available at <http://www.nature.com/reprints>

Publisher's note Springer Nature remains neutral with regard to jurisdictional claims in published maps and institutional affiliations.

Open Access This article is licensed under a Creative Commons Attribution 4.0 International License, which permits use, sharing, adaptation, distribution and reproduction in any medium or format, as long as you give appropriate credit to the original author(s) and the source, provide a link to the Creative Commons license, and indicate if changes were made. The images or other third party material in this article are included in the article's Creative Commons license, unless indicated otherwise in a credit line to the material. If material is not included in the article's Creative Commons license and your intended use is not permitted by statutory regulation or exceeds the permitted use, you will need to obtain permission directly from the copyright holder. To view a copy of this license, visit <http://creativecommons.org/licenses/by/4.0/>.

© The Author(s) 2024